PAPER

Check for updates

MgFeSiO₄ as a potential cathode material for magnesium batteries: ion diffusion rates and voltage trends†

Jennifer Heath, Hungru Chen and M. Saiful Islam (ID) *

Developing rechargeable magnesium batteries has become an area of growing interest as an alternative to lithium-ion batteries largely due to their potential to offer increased energy density from the divalent charge of the Mg ion. Unlike the lithium silicates for Li-ion batteries, $MgFeSiO_4$ can adopt the olivine structure as observed for $LiFePO_4$. Here we combine advanced modelling techniques based on energy minimization, molecular dynamics (MD) and density functional theory to explore the Mg-ion conduction, doping and voltage behaviour of $MgFeSiO_4$. The Mg-ion migration activation energy is relatively low for a Mg-based cathode, and MD simulations predict a diffusion coefficient (D_{Mg}) of 10^{-9} cm² s⁻¹, which suggest favourable electrode kinetics. Partial substitution of Fe by Co or Mn could increase the cell voltage from 2.3 V *vs.* Mg/Mg²⁺ to 2.8–3.0 V. The new fundamental insights presented here should stimulate further work on low-cost silicate cathodes for Mg batteries.

1. Introduction

The Li-ion battery currently dominates the portable energy storage market, powering mobile phones, laptop computers and electric vehicles. But the next generation of electronics will rapidly overtake the limit of what is theoretically possible with traditional Li-ion systems. While there are new approaches, such as the development of Na-ion batteries and solid-state Li-ion batteries, that could potentially offer cost, specific energy and safety advantages, there are few options to improve energy density. One strategy to improve energy density beyond the capability of Li⁺ systems is to utilise multivalent cations, specifically the Mg²⁺ ion, owing to its similar size to Li⁺.[1–6] Improvements in energy density originate from the ability to use a metal anode rather than an insertion structure. In addition, dendrite formation, which prevents the use of Li metal anodes for Li-ion batteries, does not occur with Mg metal anodes.[2]

Due to the difficulty of Mg²⁺ insertion/extraction in host structures, the choice of cathode materials for Mg batteries is limited. This is thought to be due to stronger ionic interactions and harder charge redistribution of Mg²⁺ ions in comparison to Li⁺ ions.[3] Approaches used to improve the diffusivity of Mg²⁺ ions in cathode materials have included decreasing the particle size of the cathode,[7] charge shielding of the inserted Mg²⁺

Department of Chemistry, University of Bath, Bath, BA2 7AY, UK. E-mail: m.s.islam@bath.ac.uk

† Electronic supplementary information (ESI) available. See DOI: 10.1039/c7ta03201c

ions[8,9] and redistribution of the electrons donated by Mg to transition metal clusters.[3,10–12]

Various potential cathode materials for Mg batteries have been considered, such as V_2O_5,[13–17] polymorphs of MnO_2,[18–24] molybdenum chalcogenides,[1,3,25] and spinel sulphides and oxides.[26–29] Recently, olivine-type Mg silicates have been reported to show promising cathode performance for Mg batteries, with some indication of reversible Mg intercalation.[30–36] This follows extensive work on lithium-based silicates, Li_2FeSiO_4 and Li_2MnSiO_4, as possible low-cost and stable cathodes due to the high natural abundance of silicon and the strong Si–O bonds.[37]

It has previously been reported that the olivine phase of $MgFeSiO_4$ exhibits a degree of mixing between octahedral Mg and Fe crystallographic sites.[38–40] However, ordered phases of the $MgFeSiO_4$ structure have been synthesised through high temperature methods. A synthesis temperature of up to approximately 900 °C yields a structure where Mg²⁺ occupies M2 octahedral sites and Fe²⁺ prefers M1 octahedral sites. However above this temperature, the site preference switches, with Mg²⁺ and Fe²⁺ residing in M1 and M2 positions, respectively.[38] Therefore, above 900 °C $MgFeSiO_4$ can be synthesised with a structure analogous to $LiFePO_4$, where the Mg²⁺ ions form one-dimensional channels along the *c*-axis.

In previous studies, Mg²⁺ has been inserted into disordered olivine $FePO_4$ with a measured capacity of only ~13 mA h g⁻¹. This poor performance was found to be linked to surface amorphisation that prevented the electrochemical reaction from penetrating the bulk, rather than poor Mg²⁺ mobility in the structure.[41] A first-principles study on the magnesium silicates reports the redox and thermodynamic behaviour of these

compounds,[33] revealing a similarity between lithium- and magnesium-insertion processes. However, these calculations did not consider kinetic processes, such as the transport of Mg^{2+} ions in the host lattice, which are essential to the performance of ion intercalation electrodes.

It is well established that the underlying transport and electronic properties of battery cathode materials are crucial to the greater understanding of their electrochemistry, but are not fully characterised for $MgFeSiO_4$. Here we investigate the solid-state features that influence the electrochemical performance of ordered $MgFeSiO_4$ (with a structure analogous to olivine $LiFePO_4$), by employing advanced modelling methods to probe the Mg-ion transport properties and voltage trends from transition metal doping.

2. Methods

The methods used here are well established and detailed elsewhere.[42,43] Previous studies on inorganic solids have successfully applied these potential-based methods, including olivine-structured $LiFePO_4$ and $NaFePO_4$ (ref. 44–46) and Li and Na silicate cathode materials.[47–50] Interactions between ions in the silicate framework were described using the Born-model framework, with a long-range coulombic term and a short-range term to model electron–electron repulsions and van der Waals interactions. The inclusion of a three-body term was necessary in order to model the angle-dependent nature of the SiO_4 unit.[47] The shell model[51] was used to account for the ionic polarisability effects. The interatomic potentials used here (listed in Table S1 in ESI†) were taken from previous studies on related oxides and silicates.[47,49,52] The Mott–Littleton approach is used to simulate the lattice relaxation around defects and migrating ions, which is incorporated within the GULP code.[53]

Molecular dynamics (MD) calculations, which introduce kinetic energy to the system by solving Newton's equations of motion for an ensemble of ions at finite temperatures, were performed using the LAMMPS code.[54] The calculations were carried out on a simulation box, with periodic boundary conditions, made up of $12 \times 6 \times 10$ unit cells, consisting of 20 160 atoms. The initial configuration of the structure contained 10% Mg vacancies (and corresponding Fe^{3+} species), which were randomly distributed. The Pedone model[55] was used for the MD simulations, which was employed successfully in recent studies on Na-ion conducting battery materials.[50,56] Three initial configurations were investigated and the results of the three structures were averaged. Simulation runs were carried out using the NVT ensemble and a time step of 2 fs for long runs of 6 ns, at temperatures in the range 300–1500 K. Pre-equilibrium runs of 4 ps with NVE and NPT ensembles were first used for stable configurations. Computer simulations have been used to investigate a range of materials for lithium and sodium batteries.[40,42,56–59]

Density functional theory (DFT) calculations were performed using a plane wave basis set implemented in the VASP code.[60] A cutoff energy of 440 eV and k-point mesh of $2 \times 4 \times 5$ were needed to converge the forces and energies. PAW potentials[61,62] and the spin-polarized generalised gradient approximation (GGA) with the PBEsol functional[63] were used. DFT+U methodology was used to account for the metal d-orbitals with an effective Hubbard $U_{eff} = U - J = 4.3, 3.9, 3.3$ and 6.0 eV ($J = 1.0$ eV) for Fe, Mn, Co and Ni, respectively.[56] A ferromagnetic arrangement of the unpaired 3d electrons was assumed. The Mg^{2+}/Mg cell voltage for the Fe^{2+}/Fe^{3+} redox couple was calculated using the following equation:

$$V = \frac{\varepsilon\{MgFeSiO_4\} - \varepsilon\{Mg_xFeSiO_4\} - (x)\mu\{Mg\}}{2x} \quad (1)$$

The chemical potential of magnesium ($\mu\{Mg\}$) was calculated using Mg metal. Such DFT techniques have been applied to other battery materials[29,42,57,59] including Li-ion silicate cathodes.[58,64]

3. Results and discussion

3.1 Structural modelling

The olivine-type structure of the cation-ordered $MgFeSiO_4$ belongs to the *Pmnb* space group (Fig. 1),[34] and consists of corner sharing FeO_6 octahedra along the *bc* plane. SiO_4 tetrahedra share corners and edges with the FeO_6 octahedra. Mg ions are located in channels along the *c*-axis. The starting point of the study was to reproduce the experimentally observed structure of $MgFeSiO_4$. A comparison between the calculated unit cell parameters based on effective potentials and those of the experimental structures is given in Table 1 (and further details on potential models are given in Table S2†).

The lattice parameters were computed to within 1% of the experimental values. Reproduction of the lattice parameters adds validity to the interatomic model used for simulating defects and Mg-ion migration.

3.2 Energetics and pathways for Na-ion migration

Examination of the intrinsic Mg-ion mobility in $MgFeSiO_4$ is of interest when considering its use as a cathode material for magnesium batteries. In the olivine structure there are three potential pathways for Mg-ion migration, as shown in Fig. 2a. The activation energies of Mg migration along these pathways in $MgFeSiO_4$ are listed in Table 2, along with the Mg–Mg distances. The activation energy is significantly lower for pathway A (parallel to the *c*-axis) than for pathways B and C. This
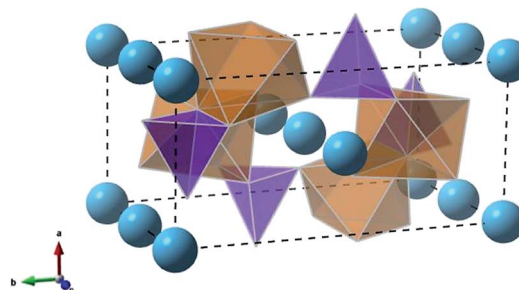

Fig. 1 Olivine-type structure of $MgFeSiO_4$ (orange octahedra: FeO_6, purple tetrahedra: SiO_4, light blue spheres: Mg^{2+} ions).

Table 1 Calculated and experimental lattice parameters and bond lengths for $MgFeSiO_4$

Parameter	Experimental[38] (Å)	Calculated (Å)	Δ (Å)
a	4.807	4.854	0.047
b	10.376	10.336	−0.040
c	6.061	6.026	−0.035
Mg–O	2.168	2.131	−0.037
Fe–O	2.125	2.140	0.015
Si–O	1.624	1.639	0.015

Table 2 Mg–Mg separations and activation energies of Mg migration in $MgFeSiO_4$

Pathway	Mg–Mg distance (Å)	E_a Mg (eV)
A	3.01	0.60
B	4.85	5.18
C	5.71	5.43
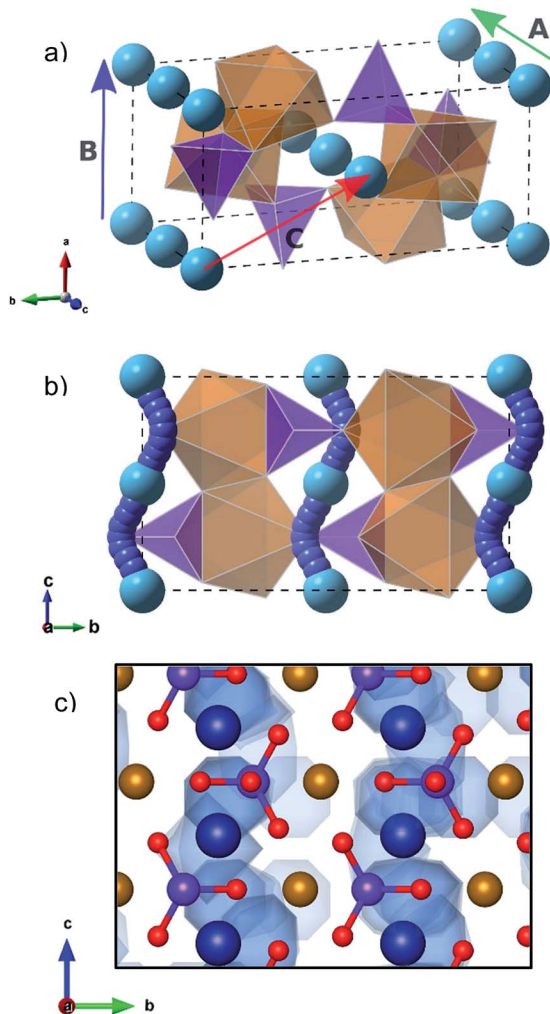
Fig. 2 (a) Mg-ion migration pathways in olivine $MgFeSiO_4$. (b) Lowest energy Mg-ion curved pathway, parallel to c-axis (brown octahedra: FeO_6, purple tetrahedra: SiO_4, blue spheres: Mg^{2+} ions); (c) Mg density plot from MD simulations showing Mg diffusion pathways (brown spheres: Fe^{2+} ions; dark blue spheres: Mg^{2+} ions; purple spheres silicon; red spheres: oxygen. Light blue channels mark diffusion pathway).

these directions. This can be rationalised by considering the structure of $MgFeSiO_4$; the distance between neighbouring Mg^{2+} ions in pathways B and C is greater than pathway A. In addition, pathway B has a smaller channel size than pathway A. Pathway C would involve migration directly past both Fe–O and Si–O bonds, both of which would contribute to the high migration energy found.

Fig. 2b shows the curved pathways along which Mg-ion migration is predicted to take place in $MgFeSiO_4$. These same migration pathways have also been simulated in olivine $LiFePO_4$,[44] and subsequently confirmed by diffraction measurements and maximum entropy studies.[65] The calculated migration energy for this pathway was 0.60 eV, just 0.05 eV higher than that calculated for $LiFePO_4$.[44]

A previous first-principles study carried out by Rong *et al.*[66] reports the migration energies of different multivalent ions in olivine $FePO_4$, layered NiO_2 and spinel Mn_2O_4. Here Mg^{2+} diffusion in the olivine structure was calculated to require approximately 0.7 eV, lower than multivalent cation diffusion in the layered and spinel structures, calculated at approximately 1.1 and 0.8 eV, respectively. The relativity low migration energies predicted for both olivine $FePO_4$ and $MgFeSiO_4$ suggest favourable Mg^{2+} ion transport in the olivine structure.

MD techniques, used here at long timescales, are well suited to examine ion motion. The curved pathways predicted using energy minimisation techniques were also generated using MD, as shown in the energy density plot in Fig. 2c.

A small degree of anti-site defects (the exchange of Mg^{2+}/Fe^{2+} on neighbouring sites) is found in the MD calculations; an example can be seen in Fig. 2c, where Mg-ion density is found near the Fe sites. These defects were anticipated given the high levels of Mg/Fe mixing in the thermodynamically stable form of $MgFeSiO_4$.[38–40] This type of defect has been reported to cause blocking of the 1D migration pathways in olivine $LiFePO_4$.[67] However, major blocking of the Mg channels was not observed in our MD simulations, which is likely to be important for reversible Mg intercalation. Hence, we predict that while anti-site defects may form causing a localised blocking effect, the Fe^{2+} ions are able to migrate back into their original sites allowing Mg^{2+} ions to diffuse through uninterrupted channels. Also there was no evidence of inter-channel hopping of the displaced Mg^{2+} ions.

The mean squared displacement (MSD) of Mg ions, $[r(t)]^2$, for $MgFeSiO_4$ is shown in Fig. 3. The MSD data can be used to derive the Mg-ion diffusion coefficient (D_{Mg}) using:

is similar to the results obtained for olivine $LiFePO_4$,[44] where the lowest energy pathway is along open channels that run parallel to the b-axis. The activation energies for pathways B and C are both prohibitively high and so Mg ion migration is not likely in

This journal is © The Royal Society of Chemistry 2017

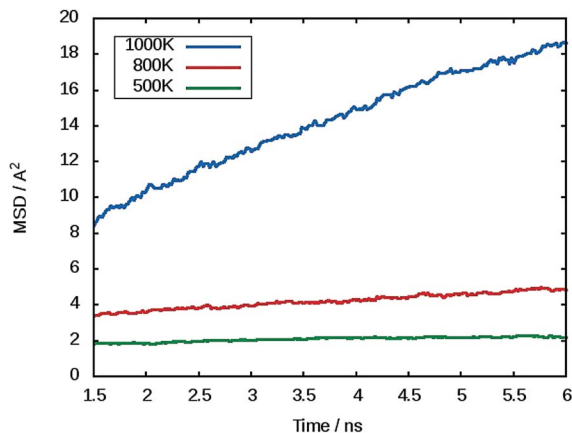*J. Mater. Chem. A*, 2017, **5**, 13161–13167 | **13163**

Fig. 3 Representative mean squared displacement (MSD) data for magnesium ions in MgFeSiO$_4$ at 500 K (green), 800 K (red) and 1000 K (blue).

$$D = \left(\frac{1}{6t}\right)\left\langle\left[r(t)\right]^2\right\rangle \qquad (2)$$

At 300 K a D_{Mg} value of 1.1×10^{-9} cm^2 s^{-1} was calculated. To our knowledge there no experimental or calculated diffusion coefficients for ordered MgFeSiO$_4$ for direct comparison. A previous study on tavorite FeSO$_4$F as a potential cathode for Mg batteries, quoted an estimated D_{Mg} in the range of 10^{-9} cm^2 s^{-1}, the same order of magnitude as observed for Li diffusion in the same structure.[68] Interestingly, Mg batteries may be more suitable for high temperature environments where the diffusion rate (and electrode kinetics) would be higher.

An Arrhenius plot for Mg^{2+} diffusion in MgFeSiO$_4$ is shown in Fig. 4, which can be used to estimate the activation energy of migration. An activation energy of 0.79 eV was derived. While this value is slightly higher than that predicted using energy minimisation, it is still relatively low for a Mg-based cathode material. This result and the prediction of D_{Mg} in the range of Li-ion cathode materials, suggests favourable Mg^{2+} intercalation kinetics for ordered MgFeSiO$_4$.
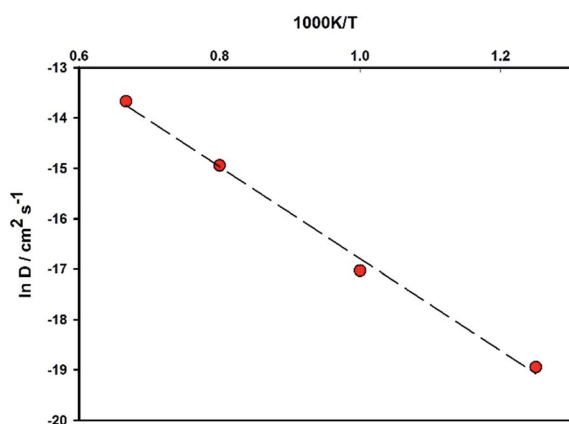

Fig. 4 Arrhenius plot of Mg-ion diffusion coefficients D_{Mg} for MgFeSiO$_4$.

3.3 Dopant substitution

Previous dopant studies on lithium-ion battery cathodes have suggested that the incorporation of dopants on certain sites could potentially improve the capacity of the material by increasing the amount of lithium available for extraction through formation of lithium interstitial defects.[47] Doping strategies could also be beneficial for magnesium-ion cathode materials. While the divalent nature of the magnesium ion offers increased energy density over monovalent lithium, many structures only allow for the de/intercalation of half of the available magnesium. The incorporation of dopants could create Mg interstitial defects that could consequently improve the capacity of the cathode material.

Here we investigate trivalent doping (Al, Ga and V) on the Si site within the MgFeSiO$_4$ structure. The doping process is described using the following equation (where M = Al, Ga or V):

$$M_2O_3 + 2Si_{Si}^{\times} + MgO \rightarrow 2M'_{Si} + Mg_i^{\cdot\cdot} + 2SiO_2 \qquad (3)$$

M^{3+} doping on the Si site is charge compensated by the formation of an Mg interstitial. We note that the alternative charge-compensation mechanism involving oxygen vacancies is less favourable by more than 4 eV. Trivalent doping on other sites in the structure would yield Fe vacancy as compensation, which would not improve the capacity or Mg diffusion in the material.

The dopant substitution reaction energies were calculated by combining the appropriate defect and lattice energy terms, listed in Table 3. Interatomic potentials used to model the corresponding binary oxides of the dopant cations were used in each case (Table S3†). This systematic approach to dopant incorporation has been applied successfully to other silicate systems.[47]

The large incorporation energies (in Table 3) for trivalent Al, Ga and V doping in MgFeSiO$_4$ to create Mg interstitials are unfavourable, and suggest a low degree of dopant solubility. Therefore, we conclude such trivalent doping of MgFeSiO$_4$ is not a viable method to improve its capacity or Mg diffusion properties.

3.4 Cell voltage trends

One challenge to overcome when developing new cathode materials for magnesium-ion batteries is to establish an adequate operating voltage (in the range of approximately 2.0–3.0 V) while simultaneously retaining a high reversible capacity.[69,70] V$_2$O$_5$ is reported to have a voltage of 2.66 V when paired with Mg/Mg^{2+}, within the appropriate range. However, as a cathode material it suffers from slow magnesium diffusion.[71]

Table 3 Calculated energies of trivalent dopant incorporation on the Si site in MgFeSiO$_4$

Dopant	Energy (eV)
Al^{3+}	5.64
Ga^{3+}	8.99
V^{3+}	8.59

13164 | *J. Mater. Chem. A*, 2017, **5**, 13161–13167

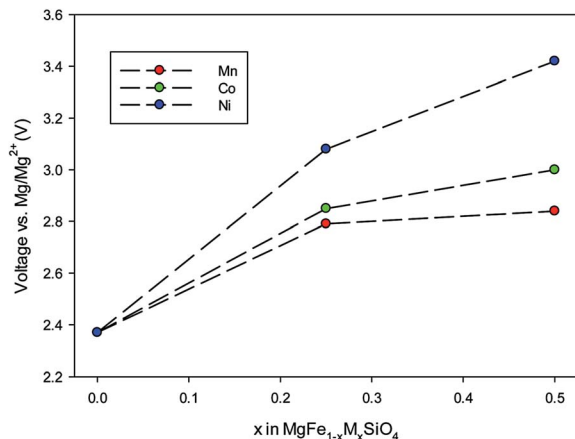This journal is © The Royal Society of Chemistry 2017

Fig. 5 Trends in cell voltage (*vs.* Mg/Mg^{2+}) as a function of increasing dopant (M = Co, Ni, Mn) on the Fe site in MgFeSiO$_4$.

Other potential cathode materials for Mg batteries have displayed voltages much lower than the optimal window, such as the Chevrel phase Mo$_6$S$_8$ and spinel MgTi$_2$S$_4$ both of which display a cell voltage of 1.2 V (ref. 1 and 26) and the cation-disordered phase of MgFeSiO$_4$ at 1.6 V.[72]

DFT was used to calculate the cell voltage of cation-ordered MgFeSiO$_4$. Similar to the potential-based calculations, the experimental structure was reproduced to a high degree of accuracy (Table S4†). To carry out the calculations relevant Mg^{2+} ions were removed from the optimised structure; various different vacancy configurations were considered and the voltage was calculated using eqn (1) with the lowest energy configuration.

First, the cell voltage of ordered MgFeSiO$_4$ was calculated to be 2.35 V *vs.* Mg/Mg^{2+}, within the operating window, and in good accord with electrochemical data showing an average voltage of 2.4 V.[34] Transition metal doping can be used to tailor the cell voltage for optimal energy density. Here we investigate how doping on the transition metal site affects the cell voltage of MgFeSiO$_4$. The voltage trends of MgFe$_{1-x}$M$_x$SiO$_4$ (M = Ni, Co and Mn) *vs.* Mg/Mg^{2+} with varied x values are shown in Fig. 5. MgFe$_{1-x}$M$_x$SiO$_4$ structures, where $x = 0.5$, follow the trend Mn (2.8 V) < Co (3.0 V) < Ni (3.4 V); we note that olivine-structured LiMPO$_4$ cathode materials follow a similar trend.[73,74] The cell voltage values of the Ni doped structures are above the adequate operating voltage for current Mg-ion electrolytes, while the Mn and Co doped structures are within this electrochemical stability window. We note that future work could include examining conversion reactions as a result of transition metal doping, a topic that goes beyond the scope of this current study.

4. Conclusions

Our fundamental study of olivine-structured MgFeSiO$_4$ as a potential cathode material for Mg batteries shows good reproduction of the experimentally observed structure and reveals key atomic-scale insights into its electrochemical properties. First, we derive an Mg-ion migration energy of 0.6 eV along the 1D channel through a curved pathway (similar to

LiFePO$_4$), and a diffusion coefficient (D_{Mg}) of 10^{-9} cm^2 s^{-1} at 300 K from large-scale MD. These ion transport results suggest favourable Mg^{2+} intercalation kinetics.

Secondly, doping of trivalent Al, Ga or V ions on Si sites is unfavourable and suggests low dopant solubility.

Finally, the DFT derived cell voltage for MgFeSiO$_4$ of 2.35 V *vs.* Mg/Mg^{2+} agrees well with the available electrochemical data. Mn or Co doping of this structure on the Fe site is predicted to increase the cell voltage to greater than 2.70 V. However, in the case of Ni doping this brings the voltage outside of the useable electrochemical stability range of current electrolytes. Overall, the fundamental insights presented here will inform the future optimisation of silicate electrodes for magnesium batteries.

References

1 D. Aurbach, Z. Lu, A. Schechter, Y. Gofer, H. Gizbar, R. Turgeman, Y. Cohen, M. Moshkovich and E. Levi, *Nature*, 2000, **407**, 724–727.

2 H. D. Yoo, I. Shterenberg, Y. Gofer, G. Gershinsky, N. Pour and D. Aurbach, *Energy Environ. Sci.*, 2013, **6**, 2265–2279.

3 E. Levi, Y. Gofer and D. Aurbach, *Chem. Mater.*, 2010, **22**, 860–868.

4 R. Van Noorden, *Nature*, 2014, **507**(7490), 26–28.

5 P. Canepa, G. Sai Gautam, D. C. Hannah, R. Malik, M. Liu, K. G. Gallagher, K. A. Persson and G. Ceder, *Chem. Rev.*, 2017, **117**, 4287–4341.

6 J. Muldoon, C. B. Bucur and T. Gregory, *Chem. Rev.*, 2014, **114**, 11683–11720.

7 N. Amir, Y. Vestfrid, O. Chusid, Y. Gofer and D. Aurbach, *J. Power Sources*, 2007, **174**, 1234–1240.

8 P. Novak and J. Desilvestro, *J. Electrochem. Soc.*, 1993, **140**, 140–144.

9 P. Novak, W. Scheifele, F. Joho and O. Haas, *J. Electrochem. Soc.*, 1995, **142**, 2544–2550.

10 E. Levi, E. Lancry, A. Mitelman, D. Aurbach, O. Isnard and D. Djurado, *Chem. Mater.*, 2006, **18**, 3705–3714.

11 E. Levi, E. Lancry, A. Mitelman, D. Aurbach, G. Ceder, D. Morgan and O. Isnard, *Chem. Mater.*, 2006, **18**, 5492–5503.

12 E. Levi, A. Mitelman, O. Isnard, M. Brunelli and D. Aurbach, *Inorg. Chem.*, 2008, **47**, 1975–1983.

13 D. B. Le, S. Passerini, F. Coustier, J. Guo, T. Soderstrom, B. B. Owens and W. H. Smyrl, *Chem. Mater.*, 1998, **10**, 682–684.

14 S. H. Lee, R. A. DiLeo, A. C. Marschilok, K. J. Takeuchi and E. S. Takeuchi, *ECS Electrochem. Lett.*, 2014, **3**, 87–90.

15 N. Y. Sa, H. Wang, D. L. Proffit, A. L. Lipson, B. Key, M. Liu, Z. X. Feng, T. T. Fister, Y. Ren, C. J. Sun, J. T. Vaughey,

This journal is © The Royal Society of Chemistry 2017

J. Mater. Chem. A, 2017, **5**, 13161–13167 | **13165**

P. A. Fenter, K. A. Persson and A. K. Burrell, *J. Power Sources*, 2016, **323**, 44–50.

16 Y. W. Cheng, Y. Y. Shao, V. Raju, X. L. Ji, B. L. Mehdi, K. S. Han, M. H. Engelhard, G. S. Li, N. D. Browning, K. T. Mueller and J. Liu, *Adv. Funct. Mater.*, 2016, **26**, 3446–3453.

17 S. Tepavcevic, Y. Z. Liu, D. H. Zhou, B. Lai, J. Maser, X. B. Zuo, H. Chan, P. Kral, C. S. Johnson, V. Stamenkovic, N. M. Markovic and T. Rajh, *ACS Nano*, 2015, **9**, 8194–8205.

18 R. G. Zhang, X. Q. Yu, K. W. Nam, C. Ling, T. S. Arthur, W. Song, A. M. Knapp, S. N. Ehrlich, X. Q. Yang and M. Matsui, *Electrochem. Commun.*, 2012, **23**, 110–113.

19 N. Kumagai, S. Komaba and H. Sakai, *J. Power Sources*, 2001, **97**, 515–517.

20 X. Q. Sun, V. Duffort, B. L. Mehdi, N. D. Browning and L. F. Nazar, *Chem. Mater.*, 2016, **28**, 534–542.

21 C. Ling, R. G. Zhang, T. S. Arthur and F. Mizuno, *Chem. Mater.*, 2015, **27**, 5799–5807.

22 K. W. Nam, S. Kim, S. Lee, M. Salama, I. Shterenberg, Y. Gofer, J. S. Kim, E. Yang, C. S. Park, S. S. Lee, W. S. Chang, S. G. Doo, Y. N. Jo, Y. Jung, D. Aurbach and J. W. Choi, *Nano Lett.*, 2015, **15**, 4071–4079.

23 L. Wang, K. Asheim, P. E. Vullum, A. M. Svensson and F. Vullum-Bruer, *Chem. Mater.*, 2016, **28**, 6459–6470.

24 R. Zhang, T. S. Arthur, C. Ling and F. Mizuno, *J. Power Sources*, 2015, **282**, 630–638.

25 L. W. F. Wan, B. R. Perdue, C. A. Apblett and D. Prendergast, *Chem. Mater.*, 2015, **27**, 5932–5940.

26 X. Q. Sun, P. Bonnick, V. Duffort, M. Liu, Z. Q. Rong, K. A. Persson, G. Ceder and L. F. Nazar, *Energy Environ. Sci.*, 2016, **9**, 2273–2277.

27 J. C. Knight, S. Therese and A. Manthiram, *ACS Appl. Mater. Interfaces*, 2015, **7**, 22953–22961.

28 C. Kim, P. J. Phillips, B. Key, T. H. Yi, D. Nordlund, Y. S. Yu, R. D. Bayliss, S. D. Han, M. N. He, Z. C. Zhang, A. K. Burrell, R. F. Klie and J. Cabana, *Adv. Mater.*, 2015, **27**, 3377–3384.

29 M. Liu, Z. Q. Rong, R. Malik, P. Canepa, A. Jain, G. Ceder and K. A. Persson, *Energy Environ. Sci.*, 2015, **8**, 964–974.

30 Z. Feng, J. Yang, Y. NuLi, J. Wang, X. Wang and Z. Wang, *Electrochem. Commun.*, 2008, **10**, 1291–1294.

31 Y. NuLi, Y. Zheng, Y. Wang, J. Yang and J. Wang, *J. Mater. Chem.*, 2011, **21**, 12437–12443.

32 Y. NuLi, Y. Zheng, F. Wang, J. Yang, A. I. Minett, J. Wang and J. Chen, *Electrochem. Commun.*, 2011, **13**, 1143–1146.

33 C. Ling, D. Banerjee, W. Song, M. Zhang and M. Matsui, *J. Mater. Chem.*, 2012, **22**, 13517–13523.

34 Y. Orikasa, T. Masese, Y. Koyama, T. Mori, M. Hattori, K. Yamamoto, T. Okado, Z. D. Huang, T. Minato, C. Tassel, J. Kim, Y. Kobayashi, T. Abe, H. Kageyama and Y. Uchimoto, *Sci. Rep.*, 2014, **4**, 5622.

35 Y. Zheng, Y. NuLi, Q. Chen, Y. Wang, J. Yang and J. Wang, *Electrochim. Acta*, 2012, **66**, 75–81.

36 T. Mori, T. Masese, Y. Orikasa, Z. D. Huang, T. Okado, J. Kim and Y. Uchimoto, *Phys. Chem. Chem. Phys.*, 2016, **18**, 13524–13529.

37 M. S. Islam, R. Dominko, C. Masquelier, C. Sirisopanaporn, A. R. Armstrong and P. G. Bruce, *J. Mater. Chem.*, 2011, **21**, 9811–9818.

38 S. A. T. Redfern, G. Artioli, R. Rinaldi, C. M. B. Henderson, K. S. Knight and B. J. Wood, *Phys. Chem. Miner.*, 2000, **27**, 630–637.

39 S. Chatterjee, S. Sengupta, T. Saha-Dasgupta, K. Chatterjee and N. Mandal, *Phys. Rev. B: Condens. Matter Mater. Phys.*, 2009, **79**, 115103.

40 S. Chatterjee, S. Bhattacharyya, S. Sengupta and T. Saha-Dasgupta, *Phys. Chem. Miner.*, 2011, **38**, 259–265.

41 R. G. Zhang and C. Ling, *ACS Appl. Mater. Interfaces*, 2016, **8**, 18018–18026.

42 M. S. Islam and C. A. J. Fisher, *Chem. Soc. Rev.*, 2013, **43**, 185–204.

43 C. R. A. Catlow, *Computer Modelling in Inorganic Crystallography*, Academic Press, 1997.

44 M. S. Islam, D. J. Driscoll, C. A. J. Fisher and P. R. Slater, *Chem. Mater.*, 2005, **17**, 5085–5092.

45 C. Tealdi, J. Heath and M. S. Islam, *J. Mater. Chem. A*, 2016, **4**, 6998–7004.

46 R. Tripathi, S. M. Wood, M. S. Islam and L. F. Nazar, *Energy Environ. Sci.*, 2013, **6**, 2257–2264.

47 N. Kuganathan and M. S. Islam, *Chem. Mater.*, 2009, **21**, 5196–5202.

48 C. A. J. Fisher, N. Kuganathan and M. S. Islam, *J. Mater. Chem. A*, 2013, **1**, 4207–4214.

49 A. R. Armstrong, N. Kuganathan, M. S. Islam and P. G. Bruce, *J. Am. Chem. Soc.*, 2011, **133**, 13031–13035.

50 J. C. Treacher, S. M. Wood, M. S. Islam and E. Kendrick, *Phys. Chem. Chem. Phys.*, 2016, **18**, 32744–32752.

51 B. G. Dick and A. W. Overhauser, *Phys. Rev.*, 1958, **112**, 90–103.

52 G. V. Lewis and C. R. A. Catlow, *J. Phys. C: Solid State Phys.*, 1985, **18**, 1149–1161.

53 J. D. Gale and A. L. Rohl, *Mol. Simul.*, 2003, **29**, 291–341.

54 S. Plimpton, *J. Comput. Phys.*, 1995, **117**, 1–19.

55 A. Pedone, G. Malavasi, M. C. Menziani, A. N. Cormack and U. Segre, *J. Phys. Chem. B*, 2006, **110**, 11780–11795.

56 S. M. Wood, C. Eames, E. Kendrick and M. S. Islam, *J. Phys. Chem. C*, 2015, **119**, 15935–15941.

57 A. R. Armstrong, C. Lyness, P. M. Panchmatia, M. S. Islam and P. G. Bruce, *Nat. Mater.*, 2011, **10**, 223–229.

58 C. Eames, A. R. Armstrong, P. G. Bruce and M. S. Islam, *Chem. Mater.*, 2012, **24**, 2155–2161.

59 Y. Yuan, C. Zhan, K. He, H. Chen, W. Yao, S. Sharifi-Asl, B. Song, Z. Yang, A. Nie, X. Luo, H. Wang, S. M. Wood, K. Amine, M. S. Islam, J. Lu and R. Shahbazian-Yassar, *Nat. Commun.*, 2016, **7**, 13374.

60 G. Kresse and J. Furthmuller, *Phys. Rev. B: Condens. Matter Mater. Phys.*, 1996, **54**, 11169–11186.

61 G. Kresse and D. Joubert, *Phys. Rev. B: Condens. Matter Mater. Phys.*, 1999, **59**, 1758–1775.

62 P. E. Blochl, *Phys. Rev. B: Condens. Matter Mater. Phys.*, 1994, **50**, 17953–17979.

63 J. P. Perdew, K. Burke and M. Ernzerhof, *Phys. Rev. Lett.*, 1996, **77**, 3865–3868.

64 M. E. Arroyo-de Dompablo, M. Armand, J. M. Tarascon and U. Amador, *Electrochem. Commun.*, 2006, **8**, 1292–1298.

13166 | *J. Mater. Chem. A*, 2017, **5**, 13161–13167

This journal is © The Royal Society of Chemistry 2017

65 S.-I. Nishimura, G. Kobayashi, K. Ohoyama, R. Kanno, M. Yashima and A. Yamada, *Nat. Mater.*, 2008, **7**, 707–711.

66 Z. Q. Rong, R. Malik, P. Canepa, G. S. Gautam, M. Liu, A. Jain, K. Persson and G. Ceder, *Chem. Mater.*, 2015, **27**, 6016–6021.

67 C. Tealdi, C. Spreafico and P. Mustarelli, *J. Mater. Chem.*, 2012, **22**, 24870–24876.

68 J. D. Wu, G. H. Gao, G. M. Wu, B. Liu, H. Y. Yang, X. W. Zhou and J. C. Wang, *Phys. Chem. Chem. Phys.*, 2014, **16**, 22974–22978.

69 M. M. Huie, D. C. Bock, E. S. Takeuchi, A. C. Marschilok and K. J. Takeuchi, *Coord. Chem. Rev.*, 2015, **287**, 15–27.

70 P. Saha, M. K. Datta, O. I. Velikokhatnyi, A. Manivannan, D. Alman and P. N. Kumta, *Prog. Mater. Sci.*, 2014, **66**, 1–86.

71 G. Gershinsky, H. D. Yoo, Y. Gofer and D. Aurbach, *Langmuir*, 2013, **29**, 10964–10972.

72 Z. Z. Feng, J. Yang, Y. N. NuLi and J. L. Wang, *J. Power Sources*, 2008, **184**, 604–609.

73 A. Yamada, M. Hosoya, S. C. Chung, Y. Kudo, K. Hinokuma, K. Y. Liu and Y. Nishi, *J. Power Sources*, 2003, **119**, 232–238.

74 C. Masquelier and L. Croguennec, *Chem. Rev.*, 2013, **113**, 6552–6591.

This journal is © The Royal Society of Chemistry 2017

J. Mater. Chem. A, 2017, **5**, 13161–13167 | **13167**